Synergistic Regulation of Coordination Sites of Co_3O_4 by Selective Doping for Efficient Water Oxidation

Zhiyu Shao,[a] Xia Gao,[a] Qian Zhu,[a] Weifeng Zhao,[a] Xiaotian Wu,[a] Keke Huang*,[a] and Shouhua Feng [a]

Experimental Section

Synthesis of Co_3O_4, Al-Co_3O_4, and In-Co_3O_4

Typically, 3 mmol of $Co(NO_3)_2 \cdot 6H_2O$ (0.87 g) was dissolved in 25 ml ethanol to produce a clear solution. Then dry SBA-15 (0.30 g) was added to the solution. After stirring for 24 h, the solution was dried by evaporation of the solvent at 40 °C. The dried powder was grounded and impregnation was repeated one more time to prepare Co- composites. The dry powder was sintered at 550 °C for 3 h and finally the silica template was removed by stirring two times with 2 M hot NaOH solution. The resultant meso-Co_3O_4 was collected after washing with deionized water and ethanol for three times.

The synthetic methods of the samples are basically the same, but the difference lies in the addition of $Al(NO_3)_2 \cdot 9H_2O$ or $In(NO_3)_2 \cdot 4.5H_2O$ were added in the impregnation process for Al-Co_3O_4 and In-Co_3O_4.

Catalyst characterization

Powder X-ray diffraction (XRD) data was obtained by using a Rigaku D/Max 2550 diffractometer with Cu-Kα radiation testing at 40 kV and 200 mA by step scanning in the angel range of 15° to 80° with increments of $3°\cdot min^{-1}$. The morphology and structure of the samples were observed by scanning electron microscopy (SEM, JEM 7900F) and high-resolution transmission electron microscopy (HRTEM, FEI TecnaiG2 S-Twin) with a field emission gun operating at 200 kV. X-ray photoelectron spectroscopy (XPS, ESCALAB-250) was carried out with Thermo ESCA Lab 250 analyzer operating at constant analyzer power mode.

Electrochemical measurement

Electrochemical measurements were conducted at the CHI 660E electrochemical workstation (Shanghai Chenhua Apparatus, China) using a standard three-electrode system, with a rotating disk electrode (5 mm in diameter) as the working electrode, a platinum slice as the counter electrode, and a Hg/HgO as the reference electrode in 1 M KOH. The working electrode was prepared by polishing it with 50 nm α-Al_2O_3 on a polishing cloth, then dropping 20 μL of the catalyst ink and drying it naturally. The catalyst ink was made by mixing the sample and Ketjenblack in a ratio of 4 to 1 to improve the electrical conductivity of test samples, adding 1 ml of deionized water and 1 ml of isopropanol and 20 μL of

Nafion solution, and then the solution was treated with ultrasonic for half an hour to make sure samples were well dispersed. The electrode was activated and the surface bubbles of it were removed by running cyclic voltammetry (CV). The OER curve was scanned from 0.2 to 0.9 V (vs Hg/HgO) with a scan rate of 5 $mV \cdot s^{-1}$ in 1 M KOH. Electrochemical impedance spectroscopy (EIS) was obtained at 0.7 V (vs Hg/HgO) with frequencies ranging from 100 kHz to 0.1 Hz within an AC voltage of 5 mV.

Density Functional Theory Calculations.

The density function calculations were performed using Vienna ab initio simulation package (VASP) with the projector augmented-wave (PAW) method. The generalized gradient approximation (GGA) functional parametrized by Perde Burke-Ernzerh of (PBE) was employed to describe the exchange correlation potential. A plane-wave energy cutoff of 400 eV was used and the energies and forces on each atom were converged to 10-4 eV and 0.05 eV/Å, respectively. A gamma-only point was used for the Brillouin zone integrations in geometry optimization, while other calculations employed a Γ-centered k-point mesh of 5×5×3.

Co_3O_4 (311) surface model was built based on the exposed (311) surface of Co_3O_4 observed by TEM results. On the basis of pristine Co_3O_4, Three Al atoms doped into octahedral sites to represent Al-Co_3O_4, and four In

atoms doped into in octahedral and tetrahedral sites to represent Al-Co_3O_4 based on the EDX analysis. A vacuum layer of 1.5 nm was used along the c direction normal to the surface to avoid periodic interactions in all models.

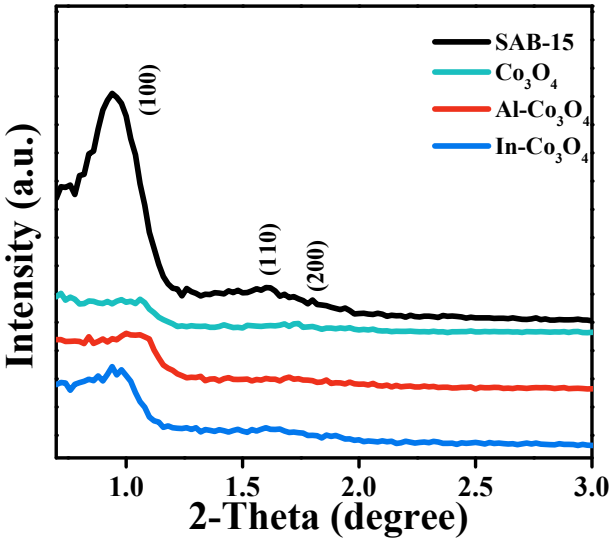

Fig. S1 Small-angle XRD patterns of SBA-15, Co_3O_4, Al-Co_3O_4, and In-Co_3O_4.

The mesoporous structures of the materials were further characterized by the small-angle XRD technique. Three well resolved diffraction peaks are observed in the XRD patterns of SBA-15. The peaks centered at 2θ = 0.94, 1.6, and 1.8° are indexed as (100), (110), (200) reflections. This is evidence of ordered two-dimensional hexagonal (p6mm) structures. The three characteristic peaks can be also detected in the patterns of the supported materials, further verifying the overall ordered mesopores of SBA-15 are well preserved after loading. Notably, the intensities of the three reflections of SBA-15 support decrease notably with loading Co_3O_4 atalysts, meaning a slight decrease in long-range periodicity order of the support pores. A careful observation of the (100) peak reveals a noticeable shift to higher 2θ values in Al-Co_3O_4, which corresponding to shrinkage of the lattice parameter.

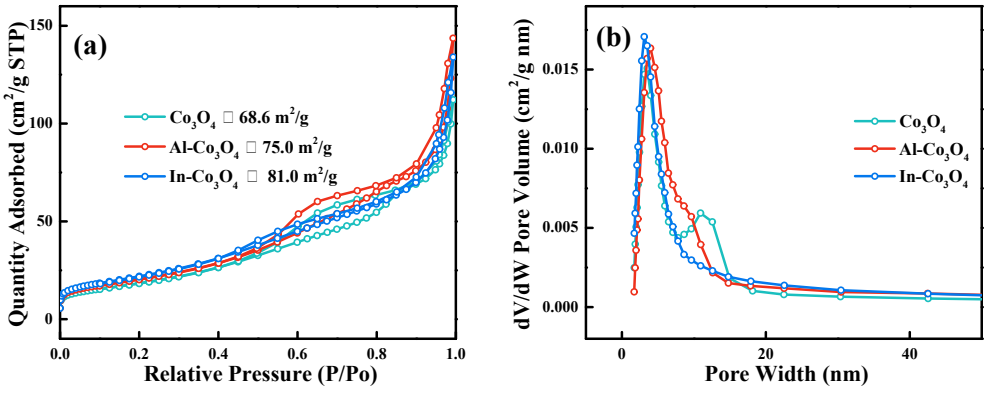

Fig. S2 (a) N_2 adsorption–desorption isotherms and (b) pore size distributions of Co_3O_4, Al-Co_3O_4,

and In-Co_3O_4.

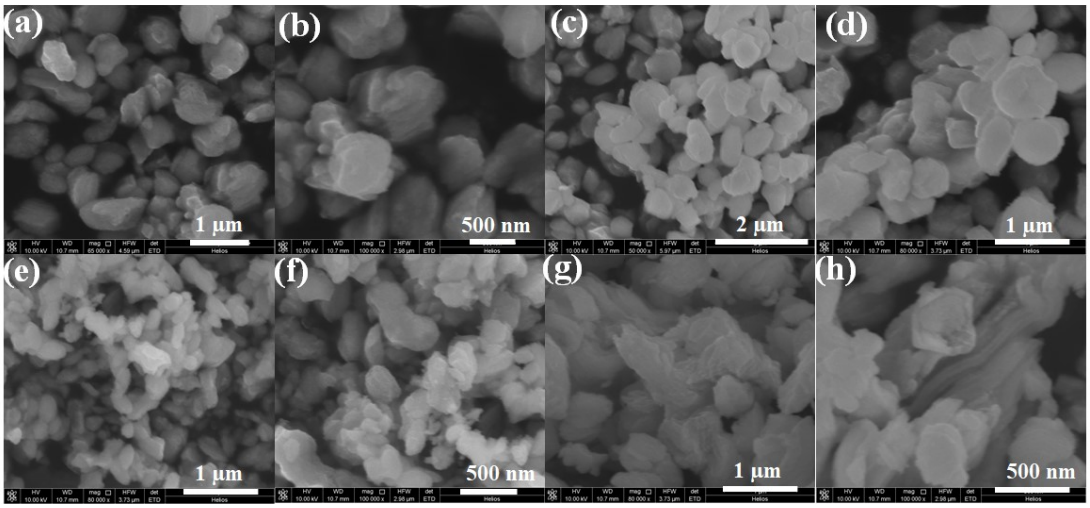

Fig. S3 SEM images of (a-b) SBA-15, (c-d) Co_3O_4, (e-f) Al- Co_3O_4, and (g-h) In- Co_3O_4.

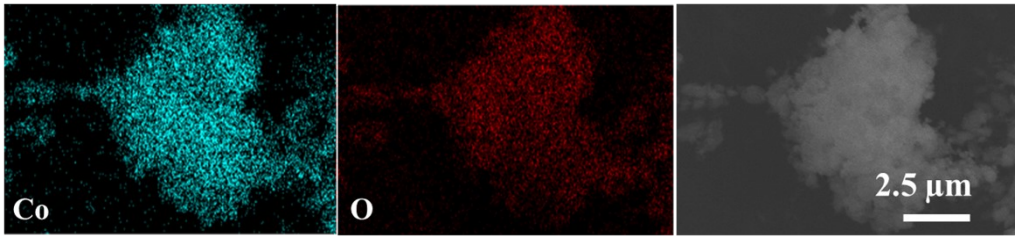

Fig. S4 EDS elemental mapping images of Co_3O_4.

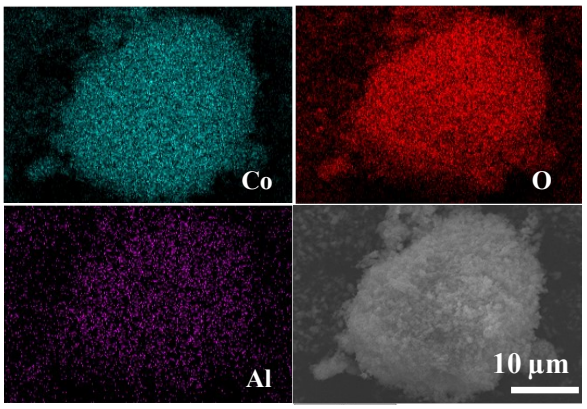

Fig. S5 EDS elemental mapping images of Al-Co_3O_4.

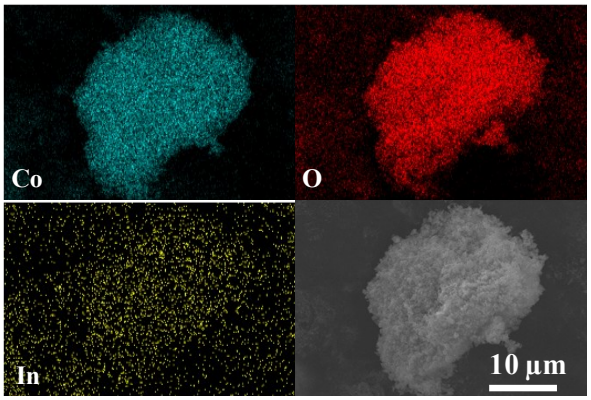

Fig. S6 EDS elemental mapping images of In-Co_3O_4.

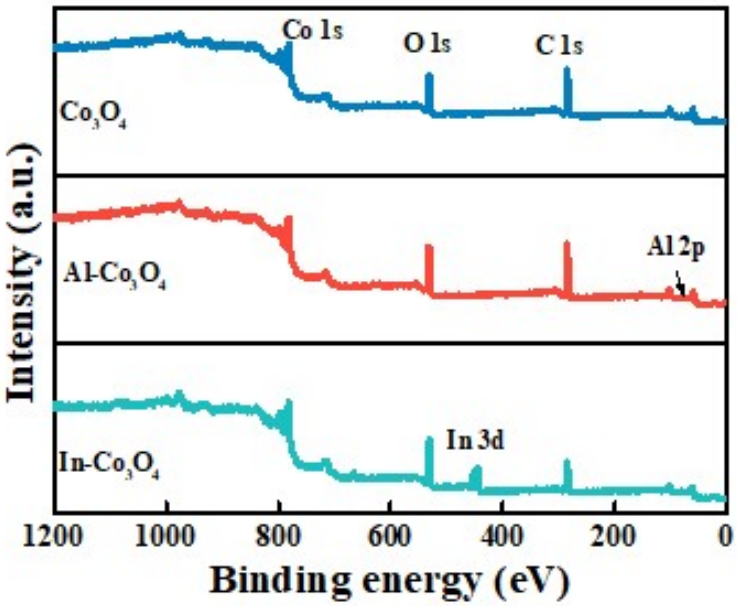

Fig. S7 XPS surface analysis of pure Co_3O_4, Al-Co_3O_4, and In-Co_3O_4.

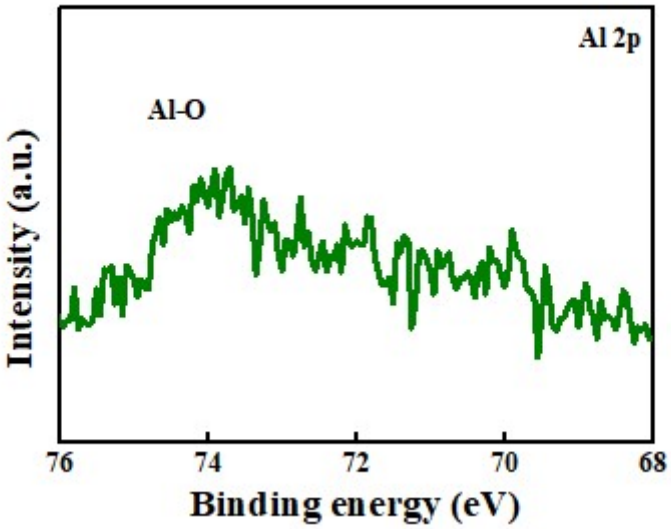

Fig. S8 XPS spectra of Al 2p of Al-Co_3O_4.

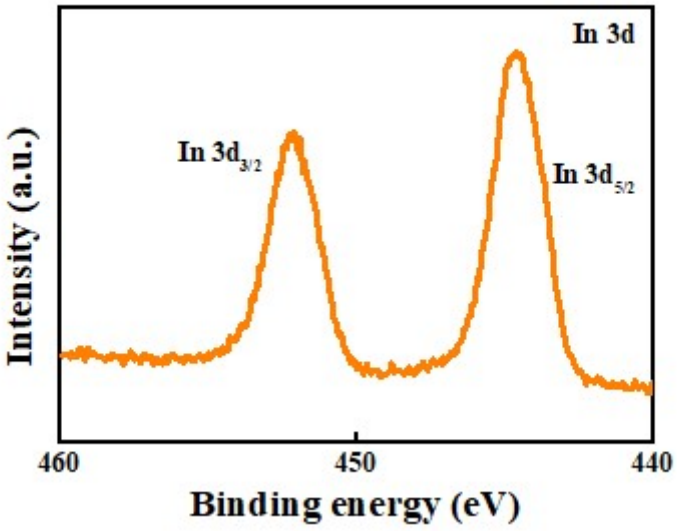

Fig. S9 XPS spectra of In 3d of In-Co_3O_4.

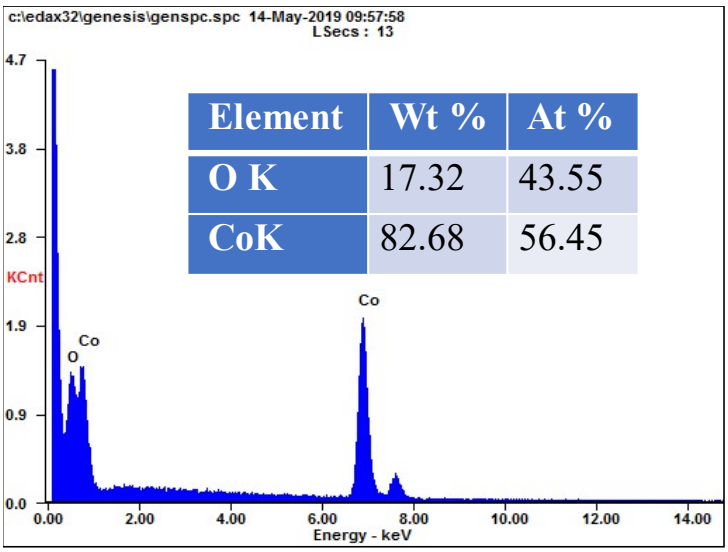

Fig. S10 EDX analysis for Co_3O_4.

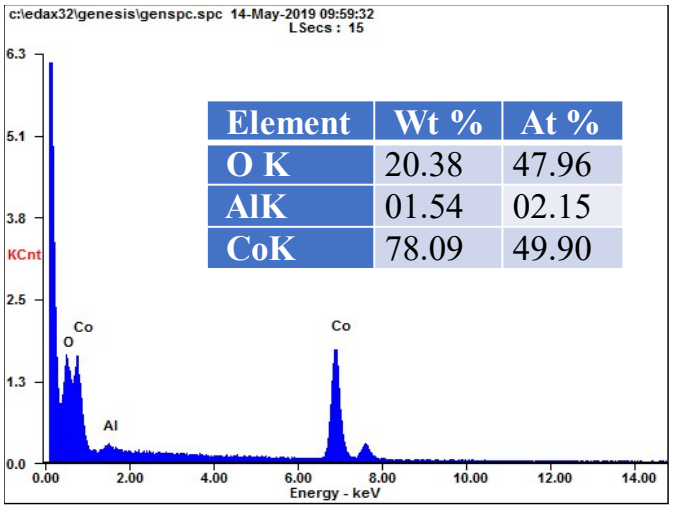

Fig. S11 EDX analysis for Al-Co_3O_4.

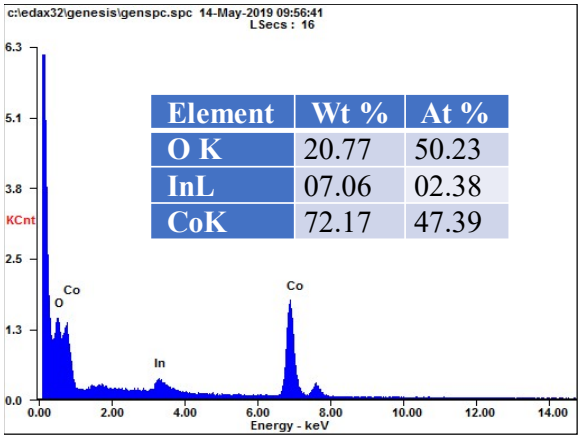

Fig. S12 EDX analysis for In-Co_3O_4.

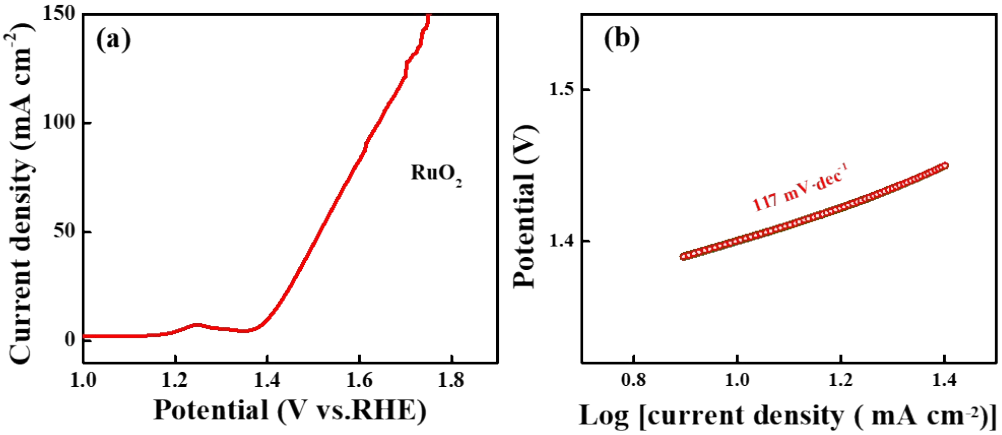

Fig. S13 (a) LSV curve and (b) corresponding Tafel plot of commercial RuO_2.

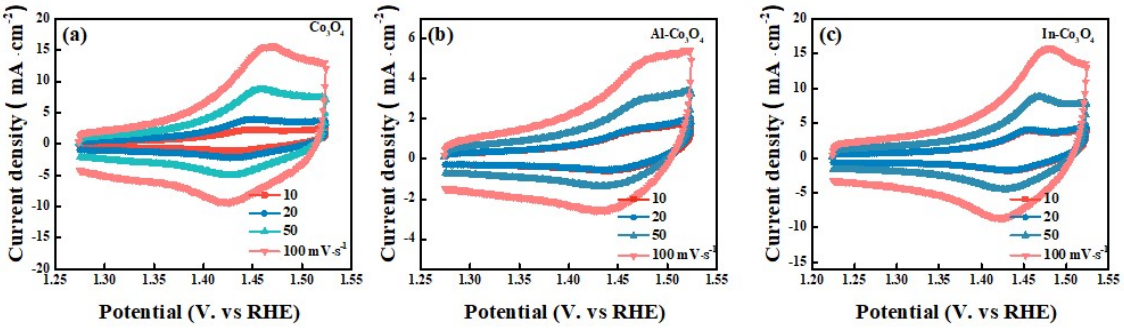

Fig. S14 CV curves with at different scanning rates of Co_3O_4, Al-Co_3O_4, and In-Co_3O_4.

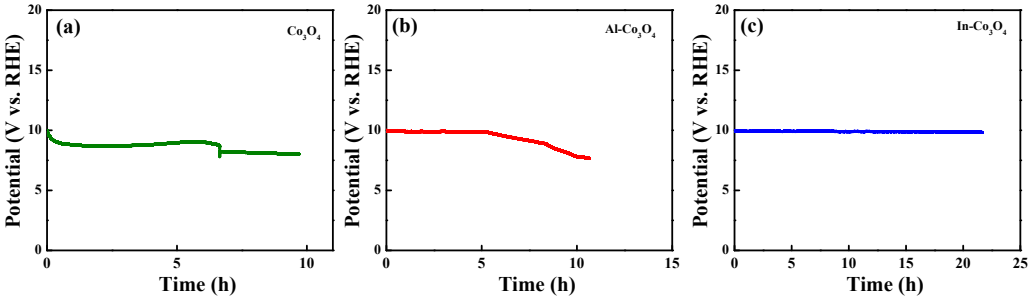

Fig. S15 Chronoamperometric curves for Co_3O_4, Al-Co_3O_4, and In-Co_3O_4.

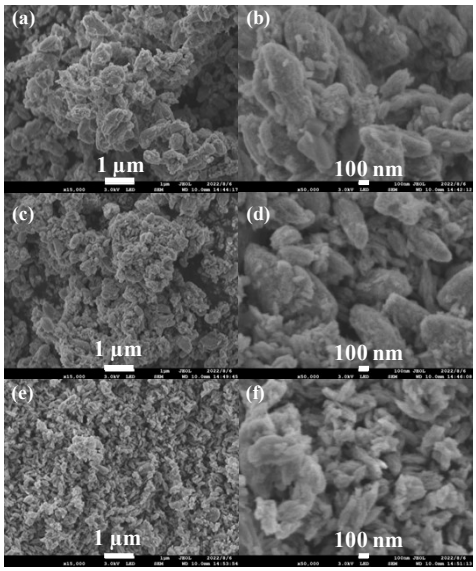

Fig. S16 SEM images of (a & b) Co_3O_4, (c & d) Al-Co_3O_4, and (e & f) In-Co_3O_4 at two different magnifications.

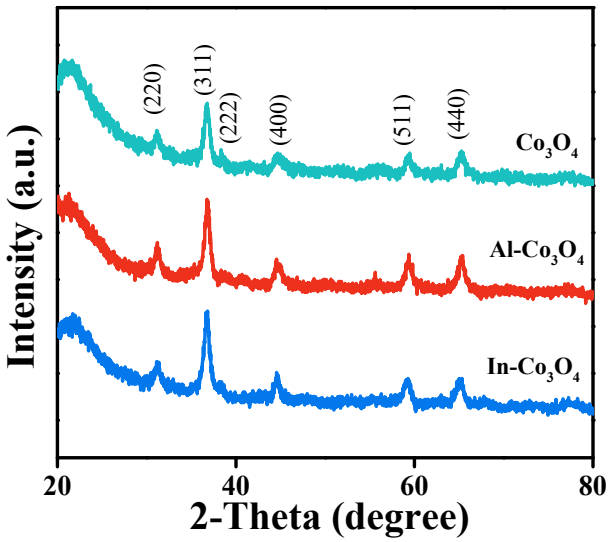

Fig. S17 XRD patterns of the electrocatalysts Co_3O_4, Al-Co_3O_4, and In-Co_3O_4.

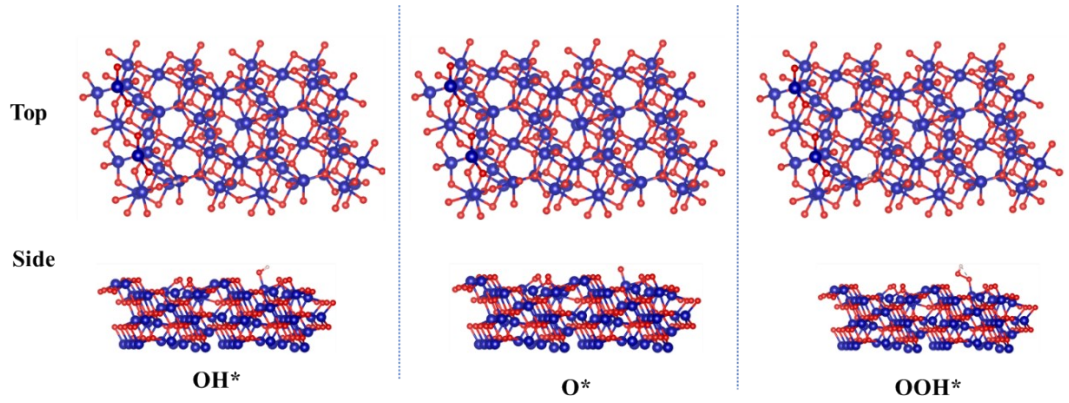

Fig. S18 The optimized configurations of Co_3O_4 chemisorption of OH*, O*, and OOH* intermediates.

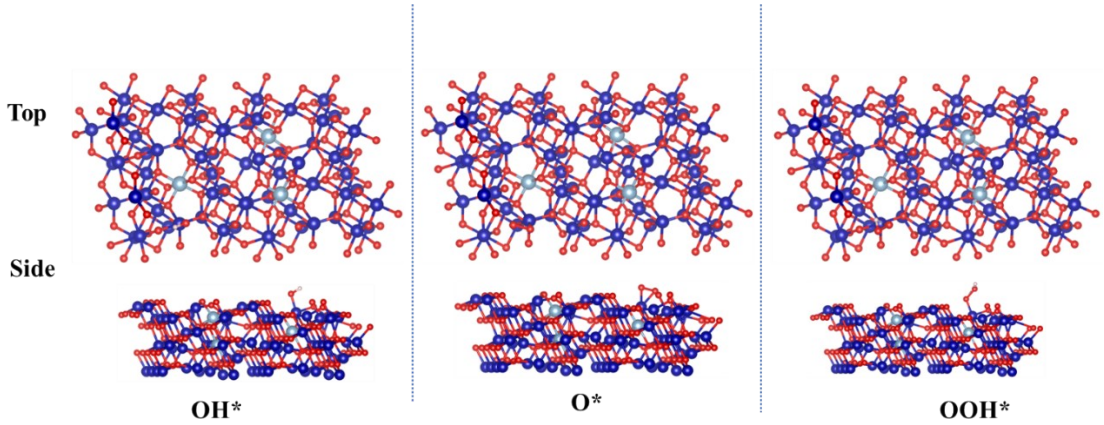

Fig. S19 The optimized configurations of Al-Co_3O_4 chemisorption of OH*, O*, and OOH* intermediates.

Table S1 Comparison of the OER activity of as-prepared catalyst with that of some recently reported electrocatalysts.

Catalyst	Current density ($mA \cdot cm^{-2}$)	Overpotential (mV)	Tafel slope ($mV \cdot dec^{-1}$)	Electrolyte	Reference
In-Co_3O_4	10	340	74	1 M KOH	**This work**
$CoCo_2O_4$/NCNTs	10	350	104	0.1 M KOH	*Angew. Chem. Int. Ed.*2022,61, e2021146
$Zn_xNi_{1-x}Co_2O_4$ /NCNTS	10	410	118	0.1 M KOH	*Angew. Chem. Int. Ed.* **2020**, *59,* 6492-6499
$La_{0.5}Sr_{0.5}MnO_3$ + 20 ALD cycles of Co_3O_4	10	470	82	0.1 M KOH	*Nano Energy.* **2020**, *71,* 104564
$MnCo_2O_4$	10	400	90	0.1 M KOH	*Angew. Chem. Int. Ed.* **2017**, *56*, 14977-14981
$CoFe_2O_4$@N-CNF	10	349	80	0.1 M KOH	*Adv. Sci.* **2017**, *4*, 1700226
Co/Co_3O_4@PGS	10	350	76	0.1 M KOH	*Adv. Energy Mater.* **2018**, *8*, 1702900
$Co_{2.25}Fe_{0.75}O_4$	10	350	50	1.0 M KOH	*J. Mater. Chem. A 2021, 9,25381-25390.*
Fe_3C/$CoFe_2O_4$@CNFs-1.5	10	340	83	0.1 M KOH	*Chem. Eng. J.* **2021**, *424*, 130460.
V-LCO/Co_3O_4	10	354	73	1.0 M KOH	*Nano Lett.* **2021**, *21*, 8166−8174
V-LCO	10	371	148	1.0 M KOH	*Nano Lett.* **2021**, *21*, 8166−8174
Co_3O_4	10	522	192	1.0 M KOH	*Nano Lett.* **2021**, *21*, 8166−8174
LCO	10	500	219	1.0 M KOH	*Nano Lett.* **2021**, *21*, 8166−8174